Article

Not peer-reviewed version

Performance of Hydrotreated Vegetable Oil–Diesel Blends: Ignition and Combustion Insights

Hubert Kuszewski *, Artur Jaworski, Dariusz Szpica

Posted Date: 17 October 2025

doi: 10.20944/preprints202510.1264.v1

Keywords: hydrotreated vegetable oil; ignition delay; diesel engine; combustion; derived cetane number

 doi:10.20944/preprints202510.1264.v1

Article

Performance of Hydrotreated Vegetable Oil–Diesel Blends: Ignition and Combustion Insights

Hubert Kuszewski [1,*], Artur Jaworski [1] and Dariusz Szpica [2]

[1] Faculty of Mechanical Engineering and Aeronautics, Rzeszow University of Technology, Powstancow Warszawy Ave. 12, 35-959 Rzeszow, Poland

[2] Faculty of Mechanical Engineering, Bialystok University of Technology, 45C Wiejska Str., 15-351 Bialystok, Poland

* Correspondence: hkuszews@prz.edu.pl; Tel.: +48 17 865 15 82

Abstract

Hydrotreated vegetable oil (HVO) is a second-generation biofuel with physicochemical properties similar to conventional diesel. Composed mainly of n-paraffins, it offers favorable autoignition characteristics. Produced by hydrotreating vegetable oils or animal fats, including waste sources such as used cooking oil, HVO contributes to lower greenhouse gas emissions and waste utilization. Thanks to its similarity to diesel, it can be used directly or in blends without engine modifications. Blending reduces fossil fuel use and pollutant emissions while maintaining engine performance. This study investigates the autoignition behavior of diesel, neat HVO, and HVO–diesel blends containing 25%, 50%, and 75% HVO by volume. Experiments were conducted in a constant-volume combustion chamber at 550 °C and 650 °C to simulate engine-relevant conditions. Autoignition quality was assessed using ignition delay, combustion delay, average and maximum pressure rise rate, maximum pressure rise, apparent heat release rate, and derived cetane number. The results show that higher HVO content increases the sensitivity of ignition delay, combustion delay, and average pressure rise rate to lower chamber temperature. In addition, a linear increase in derived cetane number was observed with increasing HVO concentration, providing new insights into ignition and combustion behavior of renewable fuel blends.

Keywords: hydrotreated vegetable oil; ignition delay; diesel engine; combustion; derived cetane number

1. Introduction

In light of growing pressure to cut emissions of greenhouse gases and air pollutants, the transportation sector—particularly road and maritime transport—is facing the challenge of gradually phasing out conventional fossil fuels. One of the most promising solutions in this context is to implement second-generation renewable fuels, such as hydrotreated vegetable oil (HVO) [1–3]. HVO is a synthetic biofuel obtained from fats of plant and animal origin, that undergo a hydrotreatment process, yielding hydrocarbons with molecular structures resembling those of conventional diesel [4–6].

Compared to conventional biodiesel, HVO exhibits a number of advantageous operational and environmental properties [7,8]. Most notably, it contains no oxygen in its molecular structure, which results in improved oxidative stability and a higher heating value. In addition, the combustion process of HVO is cleaner—reduced output of particulate matter, unburned hydrocarbons and carbon monoxide are typically observed [9,10].

Importantly, HVO may be obtained from various types of waste-derived feedstocks, including used cooking oil, which significantly lowers its carbon intensity and limits overlap with the food industry [11].

 doi:10.20944/preprints202510.1264.v1

Despite its numerous advantages, the full substitution of diesel by HVO in current transport infrastructure is not always technically or economically feasible. Consequently, growing interest is directed toward the application of diesel–HVO mixtures, which support progressive fuel decarbonization while maintaining compatibility with currently operated diesel engines [12,13].

In the context of implementing HVO and HVO–diesel blends in real-world applications, logistical and regulatory considerations also play a significant role. As a paraffinic fuel, HVO complies with the requirements of [14], which allows it to be used in modern vehicles without modifications to the fuel system—provided that it is approved by the engine manufacturer. In the case of HVO–diesel blends, it becomes essential to understand the interactions between fuel components, as these can influence not only the combustion process but also key physicochemical properties such as viscosity, density, and flash point. Properly selected blend ratios can result in a fuel with optimized ignition characteristics and a more favorable environmental balance than conventional diesel, without compromising performance. This approach represents a compromise between the goal of reducing emissions and the need to maintain continuity in existing fuel and engine infrastructure.

A critical parameter of fuel that requires evaluation—especially in the context of diesel engine operation with blended fuels—is its autoignition behavior. A shorter ignition delay period helps limit the volume of fuel that builds up in the combustion chamber during this stage, consequently lowering the pressure rise rate after ignition. As a result, mechanical stress on components of the crank-piston assembly is lowered, contributing positively to engine durability. Typically, this contributes to lowering maximum combustion temperatures, thereby decreasing nitrogen oxides (NO_x) emissions. A more detailed discussion of the influence of ignition delay on diesel engine operating processes can be found in [15–18].

In light of the above, a thorough examination of fuel autoignition behavior becomes particularly important from both operational and environmental perspectives. Research in this area can contribute to a deeper understanding of combustion processes in engines fueled with both conventional and renewable fuels, with particular emphasis on HVO, which is currently the focus of numerous studies.

Fuel autoignition behavior is most often evaluated using the cetane number (CN) or its derived form (DCN), as defined by applicable testing protocols [19, 20]. However, measuring CN using a test engine, as described in [21, 22], is complex and costly. As a result, CN data for fuels that are less common than diesel or biodiesel—such as HVO—are less readily available. It is worth noting, however, that HVO does not exhibit issues typically associated with certain alternative fuels, such as reduced lubricity or the risk of damage to injection systems. Given its physicochemical profile, which closely resembles that of diesel, HVO can be safely used within standard testing procedures. The role of CN in shaping engine performance characteristics has been thoroughly addressed in the literature [23–27], highlighting the importance of this parameter in evaluating how a fuel's autoignition behavior affects engine operation in diesel systems.

Instead of a test engine, the constant-volume combustion chamber (CVCC) approach is now more frequently applied to evaluate the autoignition properties of fuels under controlled laboratory conditions. In this context, the concept of DCN is applied. Studies focused on the DCN utilize correlations between ignition delay time and the cetane index assigned to the fuel [25,28–30]. Standardized procedures for determining DCN are described in [31–35]. In some standards, for example [32, 33], DCN is determined solely from the experimentally obtained ignition delay. In contrast, methods outlined in [34,35] also account for what is known as combustion delay, which is discussed in more detail in [36,37]. A distinctive feature of instruments used for standardized DCN determination is their ability to perform measurements under strictly controlled and repeatable conditions. This enables precise analysis of how various fuel delivery variables—including injection pressure [36, 38] and initial chamber temperature [37,38]—affect ignition delay for different types of fuels.

 doi:10.20944/preprints202510.1264.v1

Numerous studies have investigated how HVO affects performance indicators in compression-ignition engines, including [39–50]. The cited works primarily focus on powertrain efficiency and the generation of toxic exhaust compounds. These publications cover not only engine operation fueled with neat HVO but also its use in combination with other fuels, including blends with diesel. However, relatively few of the existing studies related to HVO use in compression ignition engines specifically address autoignition-related behavior of HVO and its mixtures with conventional diesel.

Some data on HVO ignition delay can be found in the work of Bjørgen et al. [40]. The authors investigated quantitative combustion-related indicators and soot behavior in spray combustion zones of three fuel categories: HVO, biodiesel (rapeseed methyl ester), and diesel. Experiments took place in a chamber with optical access under autoignition conditions, resembling thermodynamic states typically observed in engine systems. Based on these results presented, HVO exhibited the shortest ignition delay among the tested fuels over the entire range of gas-phase temperatures into which the fuel was injected (approximately 825 to 975 K). This was attributed to the highest cetane number observed for HVO.

Millo et al. [39] conducted a comparative analysis involving diesel and HVO to examine how injection-related parameters affect spray behavior along with the development of combustion. Engine tests were carried out at an engine rotational speed of 2000 rpm and three different levels of brake mean effective pressure: 8, 6, and 2 bar. For each operating point, the authors determined the ignition delay values under three different exhaust gas recirculation rates (19%, 22%, and 25%), three start of injection (SOI) timings (6, 8, and 10 CA deg aTDC), and three injection pressure (p_{ainj}) values (640, 840, and 1040 bar). The parameter values given in parentheses refer to the engine operating point corresponding to the highest load condition. The results showed that, regardless of engine operating point and parameter variation, HVO consistently exhibited shorter ignition delays compared to diesel. Moreover, the measurements indicated that injection pressure and SOI timing had the most significant impact on ignition delay at medium as well as high load conditions. Under low-load operation, SOI timing also had a noticeable influence over ignition delay.

Alkhayat et al. [51] investigated the ignition delay characteristics of HVO and its blends with ULSD (ultra-low sulfur diesel) using an ignition quality measurement device. In addition to the base fuels (HVO and ULSD), the study also included blends with HVO content of 10 %, 20 %, 30 %, 40 %, and 50 % by volume (v/v). The tests were conducted according to the procedure described in [31], and the results indicated an increase in DCN with rising HVO content within the blend. According to the authors, a clear drop was noted in ignition delay with increasing initial chamber temperature and a higher volumetric share of HVO. Furthermore, the study [51] highlighted changes in both the chemical and physical phases of ignition delay. A key factor contributing to the decrease in the physical ignition delay phase with increasing HVO content was identified as the significantly lower T90 distillation temperature of HVO compared to ULSD. A shorter chemical ignition delay observed for HVO was linked to the presence of long-chain paraffins and the lack of aromatic compounds.

Driven by the growing demand for renewable fuels used in compression ignition engines—including HVO—and the limited availability of research data in this area, this work is aimed at evaluating key ignition-related characteristics of diesel–HVO blends. The volumetric share of HVO in the blends ranged from 25 % to 75 % (v/v). Tests were also performed on the base fuels: conventional diesel designated as B7, and neat HVO. B7 refers to a standard diesel fuel, as defined by current European directives, which allows a maximum volumetric content of 7 % fatty acid methyl esters (FAME).

The novelty of this study is the systematic and extended characterization of the autoignition behavior of HVO–diesel blends across a wide blending range, conducted under controlled constant-volume chamber conditions at two distinct initial chamber temperatures. Unlike many earlier studies, which focused almost exclusively on ignition delay (ID) or derived cetane number (DCN), the present work integrates a broader set of indicators, encompassing ignition delay (ID), combustion delay (CD), pressure-rise-based parameters—average pressure rise rate (APRR), maximum pressure rise rate (MPRR), and maximum pressure rise (MPR)—as well as the apparent heat release rate (aHRR). This

 doi:10.20944/preprints202510.1264.v1

combined evaluation provides a more complete and reliable picture of how blending ratio and initial temperature affect not only the onset of ignition, but also subsequent combustion phasing and in-cylinder pressure development. Importantly, the inclusion of APRR, MPRR, and MPR offers new insights into the mechanical stresses imposed on the crank–piston assembly, which are directly linked to engine durability. For completeness and comparability, the derived cetane number (DCN) of each fuel was determined according to the standardized procedure in [34,35]. The results thus fill a gap in the limited body of data on HVO–diesel mixtures and establish a robust framework for assessing the autoignition quality of renewable fuel blends in compression ignition engines.

The findings of this investigation may offer a meaningful point of reference for further research on optimizing combustion processes in engines fueled with renewable fuel components such as HVO. Since the authors employed the ignition delay determination method described in [34,35], the findings can also provide a valuable complement to the results reported in [51], where the CVCC method was likewise applied, although using an instrument compliant with the standard specified in [31].

2. Methodological Framework

2.1. Composition and Analysis of Tested Fuels

Autoignition property tests were performed using five distinct fuel samples. Among them was a standard, commercially available diesel, which, as noted earlier, is labeled as B7 at gas stations in Europe. This designation indicates that the fuel may contain up to 7% (v/v) FAME. The same designation is used throughout this paper. The second reference fuel was HVO. For both base fuels, the majority of key chemical and physical properties were established by the authors. The results of these measurements are summarized in Table 1, which also includes information on the test equipment and measurement methods used. Distillation profiles for the B7 and HVO fuels evaluated in the present work are shown in Figure 1.

Table 1. Selected fuel composition and ignition-related properties of unblended B7 and HVO.

Measured property [unit]	Instrument	Supplier	B7 (diesel)	HVO
DCN	CID 510	Walter Herzog by PAC, USA	50.0	70.6
FAME [% (volume)]	OptiFuel	PAC, USA	6.79	–
O_2 [% (mass)]	–	–	0 [a]	0 [a]
H_2 [% (mass)]	–	–	12.86 [a]	15.16 [a]
C [% (mass)]	–	–	87.14 [a]	84.84 [a]
Total aromatics [% (mass)]	OptiFuel	PAC, USA	19.8	0 [a]
Polycyclic aromatics [% (mass)]	OptiFuel	PAC, USA	2.9	–
Tri+ aromatics [% (mass)]	OptiFuel	PAC, USA	0.2	–
Di-aromatics [% (mass)]	OptiFuel	PAC, USA	2.8	–
Mono [% (mass)]	OptiFuel	PAC, USA	16.9	–
Paraffins [% (mass)]	–	–	76.8 [b]	100 [a]
Olefins	–	–	3.4 [a]	0 [a]

 doi:10.20944/preprints202510.1264.v1

[% (mass)]				
2-EHN [ppm by mass]	OptiFuel	PAC, USA	0	-
HHV [MJ/kg]	IKA C 5000	IKA Werke GmbH & Co. KG, Germany	46.25	47.22
Density, 15 °C [g/cm³]	DMA 4500	Anton Paar GmbH, Austria	0.834	0.782
Kinematic viscosity, 40 °C [mm²/s]	HVU 472	Walter Herzog, Germany	2.81	2.90
WSD, 60 °C [µm]	PCS HFRR	PCS Instruments, UK	190.5	326.0
Water [ppm by mass]	AquaMAX KF	GR Scientific Ltd., UK	38.0	17.0
Flash point [°C]	HFP 339	Walter Herzog by PAC, USA	63.5	64.0
CFPP [°C]	FPP 5Gs	ISL, France	–21	–34
IBP [°C]	Optidist	Walter Herzog by PAC, USA	173.4	198.3

[a] Data provided by [42]. [b] Value estimated by subtracting the sum of olefins and total aromatics content from 100 %.

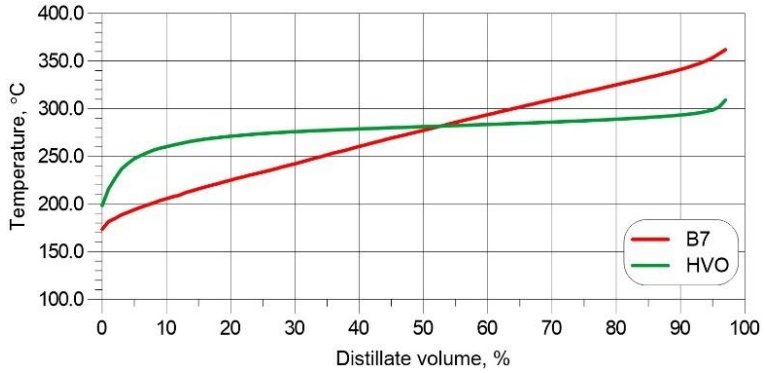

Figure 1. Distillation characteristics of B7 and HVO fuels.

Three additional fuel formulations were prepared by mixing HVO with B7 in volume-based ratios of 25%, 50%, and 75% HVO. Owing to their composition—especially the exclusive presence of paraffinic hydrocarbons in HVO—these blends show very high miscibility. Further details concerning the characteristics of HVO–diesel mixtures at different blending levels are provided in [42]. The samples were prepared under controlled conditions at 21 °C ± 1 °C for both HVO and B7. All samples were kept in hermetically sealed glass containers at the same temperature. The specific sample designations, along with their corresponding volumetric HVO content, are summarized in Table 2.

Table 2. Fuel blend designations and their volumetric composition.

Fuel designation	Volumetric composition
B7	100% B7 (standard diesel fuel)
B7-HVO-25	75% B7, 25% HVO
B7-HVO-50	50% B7, 50% HVO

 doi:10.20944/preprints202510.1264.v1

B7-HVO-75	25% B7, 75% HVO
HVO	100% HVO

2.2. Description of the Test Stand

The experimental tests were carried out using a commercially available CID 510 (Petroleum Analyzer Company; Houston, TX, USA) device, which incorporates a constant volume combustion chamber. The primary purpose of this apparatus is to determine the DCN, following the procedures specified in standards [34,35]. Similar equipment has also been used in previous studies [36,52–59]. A simplified layout of the experimental setup is presented in Figure 2, while detailed construction information is provided in [34,35]. Key components of the system—excluding the automation and control modules—include a heated constant volume combustion chamber (internal volume: 473 cm^3), a Common Rail fuel injector, a hydraulic system with a pressure intensifier, a fuel supply system, air and exhaust gas management systems, and a cooling circuit for the injector linked to an external thermostatic unit. The combustion chamber is encased in a thermally insulated jacket that ensures a stable temperature of the synthetic air. Temperature sensors are embedded in the chamber walls. Because the chamber remains continuously heated, only a short interval is needed between injections for the system to reach steady-state conditions. The initial temperature of the synthetic air inside the chamber (T_a) is assumed to be equal to the wall temperature (T_{ch}), i.e., $T_a = T_{ch}$. Details on the composition and characteristics of the synthetic air used in this study are provided in Table 3.. A high-frequency pressure transducer is installed at the base of the chamber. In the low-pressure segment of the fuel circuit—extending from the sample tank to the pressure intensifier—nitrogen gas is used to circulate the fuel at approximately 0.6 MPa. A PTFE filter is integrated into this section to remove any impurities from the fuel prior to injection.

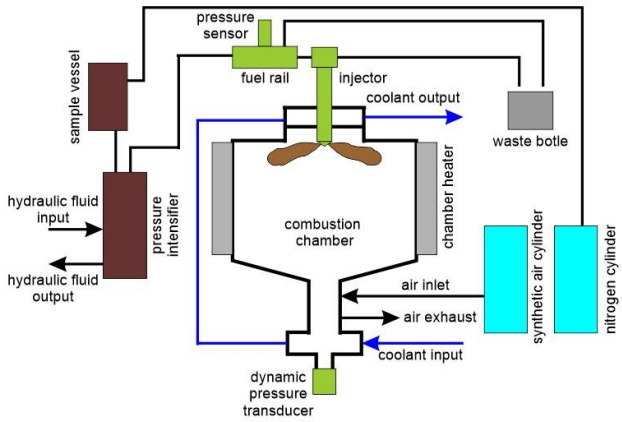

Figure 2. Simplified diagram of the test apparatus used for autoignition analysis.

Table 3. Composition breakdown of the synthetic air used during testing.

Component	Concentration*
N_2 (vol. %)	79.1% ± 0.05%
O_2 (vol. %)	20.9% ± 0.05%
H_2O (ppmv)	< 0.5
CO + CO_2 (ppmv)	< 0.1
THC (ppmv)	< 0.05
SO_2 (ppmv)	< 0.02
NO_x (ppmv)	< 0.02

 doi:10.20944/preprints202510.1264.v1

Ar (ppmv)	< 0.01

* Supplier-declared values.

The fuel injection pressure, p_{inj}, was generated by a hydraulic system incorporating a pressure intensifier. A Bosch injector (No. 0445110181) featuring a six-hole nozzle—typical of modern direct-injection engines—was installed at the upper part of the combustion chamber. The chamber's initial pressure was regulated using a static pressure sensor and a relief valve. A filtration and drainage system was also employed to protect components from contaminants. Prior to every measurement, the system was inspected for tightness, ensuring that any pressure drop did not exceed 0.75 kPa/s. The calibration process used a certified reference fuel comprising a mass-proportional blend of 40% n-hexadecane (minimum purity 99.0%) and 60% isocetane (minimum purity 98.0%). Details regarding the calibration procedure are provided in Table 4. Proper calibration of the testing apparatus is essential for standardized DCN measurement accuracy.

Table 4. Calibration parameters, setpoints, and corresponding tolerances for the auto-ignition analysis apparatus.

Parameter symbol	Unit	Value	Tolerance
t_{inj}	ms	2.5	not defined
p_{inj}	MPa	100.0	± 1.5
p_0	MPa	2.00	± 0.02
T_{ch}	°C	588.0	± 0.2
T_{co}	°C	50.0	± 2.0

2.3. Research Methodology and Data Acquisition

Each fuel variant underwent a total of 11 combustion cycles—5 initial conditioning cycles followed by 6 main measurement cycles. Throughout each cycle, the in-chamber pressure was captured using a dynamic pressure transducer operating at a sampling rate of 25 kHz. For analytical purposes, only pressure traces from the 6 main cycles were averaged and analyzed.

During these 6 cycles, the following variables were also recorded: the initial pressure in the combustion chamber, p_0, wall temperature, T_{ch}, fuel injection pressure, p_{inj}, and the MPR relative to p_0. All pressure values are given as gauge pressures, i.e., referenced to ambient pressure. During the tests, atmospheric pressure was stabilized at 98.7 kPa with fluctuations not exceeding ±0.2 kPa. The temperature of the injector cooling medium, T_{co} was also monitored and maintained at T_{co} = 50 °C consistent with calibration settings (see Table 4). The method used for determining ID, CD), and MPR is shown in Figure 3, following the standardized protocol described in [34,35].

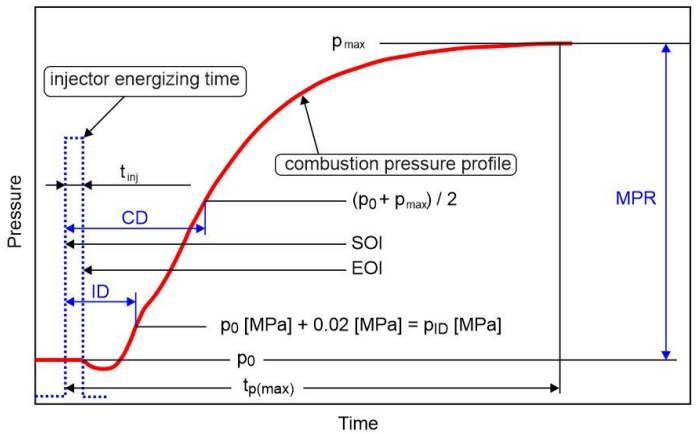

 doi:10.20944/preprints202510.1264.v1

Figure 3. Method used for determining ignition delay and combustion delay, following the procedure in [35].

Based on the pressure profiles obtained from measurements inside the combustion chamber, the APRR was determined using the formula:

$$APRR = \frac{p_{max} - p_{ID}}{t_{p(max)} - ID} \text{ [MPa/ms]} \quad (1)$$

where:

p_{max}–represents the peak pressure value measured during combustion, in MPa,

p_{ID}–pressure value recorded at the conclusion of the ignition delay phase, in MPa,

$t_{p(max)}$–denotes the time corresponding to the attainment of p_{max}, in ms,

ID–is the ignition delay duration, in ms.

The instantaneous pressure inside the combustion chamber was determined by numerically differentiating the pressure traces using a finite difference method. This approach enabled the identification and analysis of the MPRR, as illustrated in Figure 4.

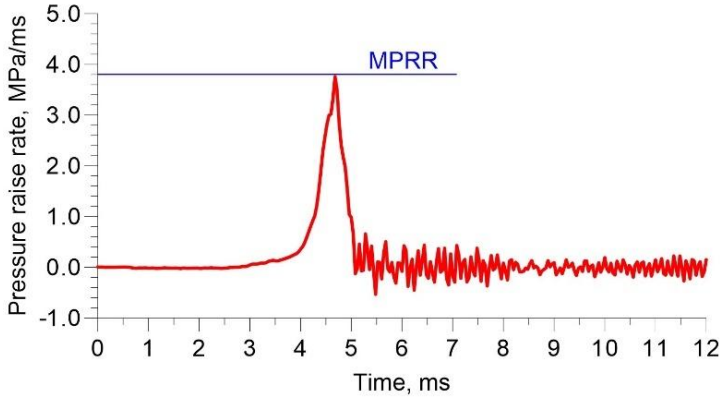

Figure 4. Method for determining the MPRR.

To examine how the initial temperature within the combustion chamber affects ignition behavior, measurements were carried out for all fuel samples listed in Table 2 at two synthetic air temperatures: T_a = 550 °C and T_a = 650 °C. These temperatures are representative of end-of-compression conditions in modern diesel engine cycles. Throughout the tests, parameters such as fuel injection pressure, p_{inj}, initial chamber pressure, p_0, injector energizing time, t_{inj}, and injector coolant temperature, T_{co}, were carefully maintained along with a constant composition of synthetic air (see Table 3), in accordance with calibration conditions (see Table 4).

The apparent heat release rate, aHRR, was estimated using a simplified formulation derived from the first law of thermodynamics:

$$\frac{dQ}{dt} = \left(\frac{\gamma}{\gamma - 1}\right) p \frac{dV}{dt} + \left(\frac{1}{\gamma - 1}\right) V \frac{dp}{dt} \quad (2)$$

where:

$\frac{dQ}{dt}$ –denotes the aHRR, in MW,

V–is the volume of the combustion chamber, which is equal to 473 cm³ (i.e., 0.000473 m³),

p–indicates the pressure inside the chamber, in Pa,

t–represents the time at which the pressure is recorded, in ms,

γ–refers to the ratio of specific heats at constant pressure and volume for the gas mixture (taken as 1.32).

In this approach, it was assumed that pressure changes result exclusively from combustion, while heat transfer between the gas and chamber walls was neglected. Moreover, the specific heat ratio γ, was treated as time-invariant. Under these conditions, the formula for aHRR is simplified. Given that the tests were carried out in a constant volume combustion chamber, the expression reduces to:

 doi:10.20944/preprints202510.1264.v1

$$\frac{dQ}{dt} = \left(\frac{1}{\gamma - 1}\right) V \frac{dp}{dt} \quad (3)$$

For the parameters ID, CD, APRR, MPRR, MPR, and DCN, the standard error of the mean (SEM) was calculated based on six combustion cycles. The uncertainty values were indicated by preceding the corresponding parameter symbol with Φ. These measurement uncertainties are summarized in Tables 5 and 6 (for T_a = 550 °C and 650 °C respectively). Both tables are included at the end of Section 3. The DCN results were obtained under calibration conditions (see Table 4), and in this case, the SEM values for each fuel sample are displayed directly on the DCN graph.

3. Experimental Results and Analysis

Figure 5 illustrates the pressure traces recorded in the combustion chamber for the tested fuels at two initial temperatures: T_a = 550 °C and 650 °C. Based on these profiles, the following parameters were evaluated in subsequent sections: ID, CD, MPR, APRR, MPRR, aHRR, and DCN. In all tests, the fuel injection pressure was maintained at p_{inj} = 100 MPa. The plots clearly demonstrate how fuel composition influences pressure rise behavior.

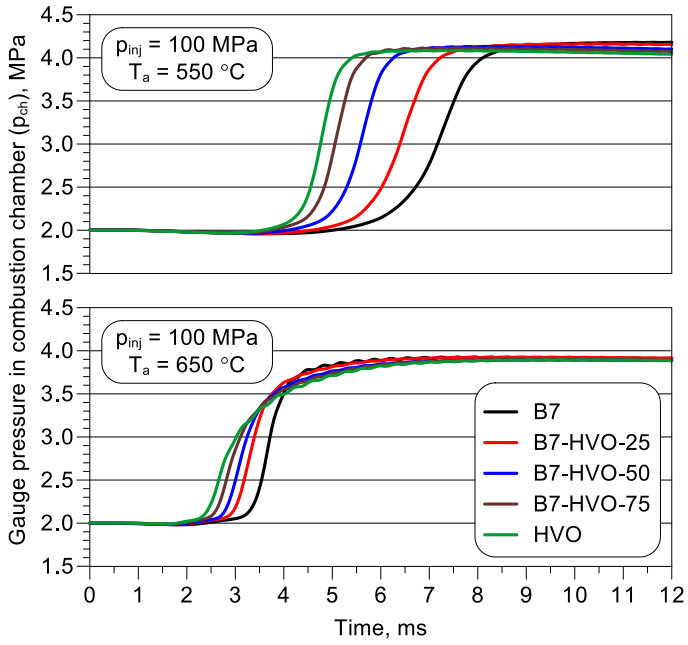

Figure 5. Pressure profiles recorded in the combustion chamber for Ta = 550 °C and 650 °C, with an injection pressure of 100 MPa.

At T_a = 550 °C, it was observed that for fuels with a higher HVO content, the combustion process proceeded more rapidly and intensely, which was reflected in the steep slope of the pressure curves. In contrast, for the B7 sample, the pressure rise was more gradual and extended over time, indicating a less intense combustion process. At T_a = 650 °C, variation in combustion intensity among the fuel variants was less pronounced, while all pressure curves exhibited a sharp and consistent rate of increase. This indicated a strong influence of the initial temperature of the surrounding air at the moment of fuel injection on the intensity of pressure rise—higher temperatures promoted faster and more vigorous combustion, regardless of the sample composition.

Figure 6 illustrates the relationship between the HVO volumetric proportion in the diesel blend and the ID, evaluated at two different initial chamber temperatures. The data indicate that, under the applied experimental conditions, a higher HVO fraction in the mixture consistently resulted in a shorter ID at both examined values of T_a. These results align with earlier observations reported in [39,40,51], which explored the autoignition characteristics of HVO and its mixtures with standard diesel. Figure 6 also reveals a notable effect of the initial temperature in the chamber on the autoignition response of the samples. A 100 °C increase in T_a led to an approximate 50% decrease in

 doi:10.20944/preprints202510.1264.v1

ID. Moreover, the results confirm that no signs of negative temperature coefficient behavior were observed throughout the studied temperature interval—in other words, ID continued to decrease with increasing T_a [60]. The identified ID patterns—especially the shorter values observed at elevated T_a—were attributed to the distinct chemical characteristics of the fuel, which significantly affected the ignition delay's chemical initiation stage [51,61,62].

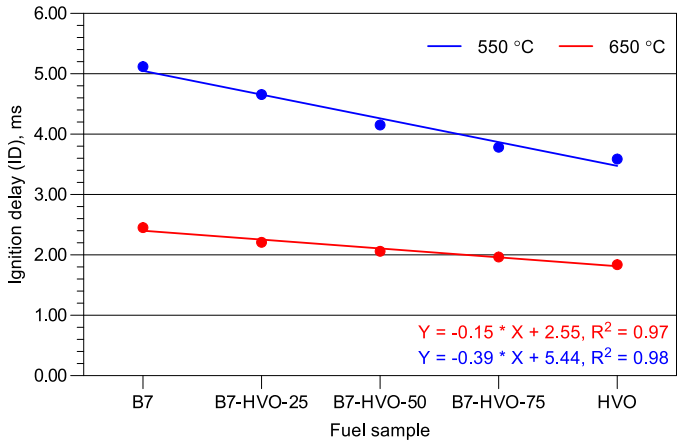

Figure 6. ID for B7, B7-HVO blends, and HVO at 550 °C and 650 °C.

Paraffinic hydrocarbons, which constitute the primary hydrocarbon structure in HVO, exhibit very good ignition properties due to their saturated molecular structure, which results in shorter ID and a more stable combustion process. Olefins, which contain double bonds, are characterized by moderate autoignition reactivity and typically exhibit medium ID values. Aromatic compounds, which are more abundant in B7 fuel, are characterized by a low cetane number and tend to exhibit the longest ignition delay due to their stable ring structure. The presence of aromatics in the fuel negatively affected the autoignition process; however, under elevated temperature conditions, the stability of the aromatic ring structure was reduced, which in turn explains the clearly shortened ID observed for B7 and its HVO blends at the higher T_a. It should also be noted that at higher temperatures, the presence of aromatics in the fuel—decreasing with increasing HVO content—became less significant, as the combustion process was increasingly dominated by the enhanced oxidation rates of H, OH, and HO_2 radicals. This explains the relatively small differences in ID values among the tested samples at elevated T_a. In summary, the predominance of paraffinic hydrocarbons and the virtual absence of aromatic species in HVO are key contributors to the enhanced ignition behavior observed for HVO and its mixtures with B7, relative to neat B7. Further insight into the ignition performance of different hydrocarbon types is provided in [51,63,64]. Additional interpretation is supported by modeling data discussed in [65,66].

As illustrated in Figure 7, the variation in the CD parameter exhibited a trend comparable to that observed for ID. The influence of HVO concentration on CD was more pronounced at the lower temperature of T_a = 550 °C, with a difference of approximately 2.5 ms between B7 and HVO. At the higher temperature of T_a = 650 °C, this difference decreased to around 0.7 ms. As defined in Figure 3, the CD value was determined not only by the maximum rate of pressure rise after autoignition, but also by the progression of pressure from the start of the recording to the moment when the maximum pressure was achieved.

 doi:10.20944/preprints202510.1264.v1

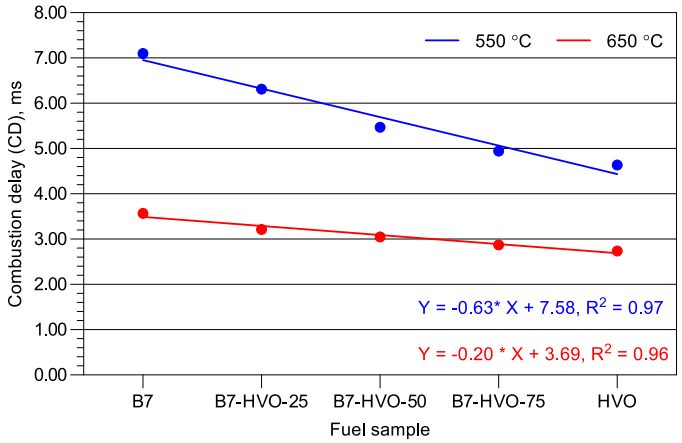

Figure 7. CD for B7, B7-HVO blends, and HVO at 550 °C and 650 °C.

The CD interval, as defined in the schematic presented in Figure 3, acts as a supplementary indicator of a fuel's tendency to autoignite and, along with ID, is employed to determine the DCN following the procedure outlined in [34,35]. The ID value corresponds to the initial phase of autoignition, commonly referred to as the cool-flame stage. As noted by Lapuerta et al. [38,59], this stage is particularly relevant in studies utilizing constant volume combustion chambers, such as the one used in this study. The formation of cool flames is mainly linked to the presence of linear and cyclic paraffins in the fuel formulation [59]. The second, main phase of autoignition begins once the surrounding temperature of the fuel droplet becomes high enough to initiate chain-branching reactions. Lapuerta et al. [59] characterized this phase based on CD and pressure evolution, noting that the CD is generally slightly longer than the true duration of the primary autoignition phase.

As shown in Figure 8, under constant volume combustion conditions, how the HVO share in the fuel mixture affects the maximum pressure rise (MPR) was observed only at the lower of the two analyzed initial temperatures, T_a. In this case, the increase in HVO content—characterized by higher chemical reactivity due to the presence of only paraffinic hydrocarbons—resulted in faster ignition, as indicated by the measured ID values. As a consequence of greater fuel accumulation during the premixed combustion phase, a noticeable rise in MPR occurred, particularly in the case of B7-HVO-75 and pure HVO.

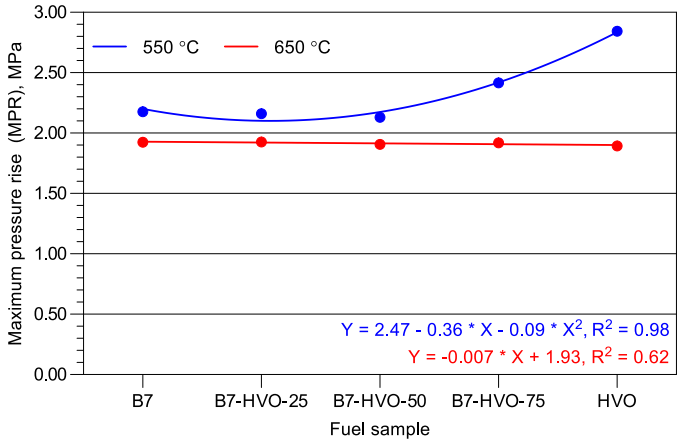

Figure 8. MPR for B7, B7-HVO blends, and HVO at 550 °C and 650 °C.

For the B7 fuel and the B7-HVO-25 and B7-HVO-50 blends, the ignition and combustion reactions proceeded more slowly due to the higher proportion of hydrocarbons with ring structures in these samples. As a result, lower MPR values were recorded. At the higher analyzed temperature,

 doi:10.20944/preprints202510.1264.v1

T_a, the chemical part of the ID was significantly shortened, and the physical part was also reduced, as the elevated temperature favored faster fuel droplet evaporation [67]. Under these conditions, the rate of chemical reactions became sufficiently high that differences in fuel reactivity no longer played a significant role. Consequently, regardless of blend composition, the MPR value remained nearly constant, indicating that a threshold had been reached at which an increase in the proportion of chain-structured hydrocarbons no longer affected the rate of fuel oxidation reactions.

Numerous studies—for example, [68–71]—indicate that reducing ignition delay, for example through pilot fuel delivery or decreasing the timing of fuel injection, lowers the amount of fuel accumulated prior to ignition. As a result, premixed combustion occurs with a lower rate of pressure increase, helping to mitigate combustion noise and NOx emissions. For this reason, an evaluation of the rate of pressure increase within the combustion chamber was carried out for the tested fuel blends at both T_a levels. The key parameter in this evaluation was the APRR, calculated using Equation 1, based on selected points from the recorded pressure traces (Figure 5). Subsequently, the MPRR was determined. This methodology has also been described and applied in the authors' previous studies, e.g., [37,58].

As illustrated in Figure 9, the APRR value for blends of HVO and diesel was influenced by the initial chamber temperature, Ta. At the lower T_a, a distinct rise in APRR occurred as the HVO share increased, despite the concurrent reduction in ID (Figure 6).

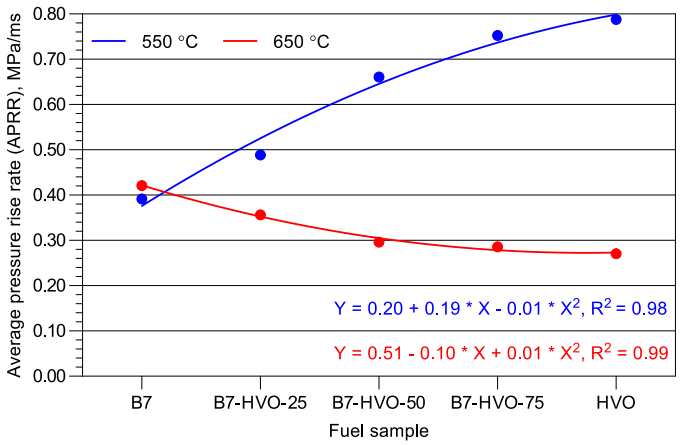

Figure 9. APRR for B7, B7-HVO blends, and HVO at 550 °C and 650 °C.

At the higher temperature, T_a = 650 °C, despite the continued decrease in ID as the HVO fraction in the fuel mixture increased (although the decrease appeared clearly smaller in this case), APRR exhibited the opposite trend—its value decreased as the HVO content increased. At the same time, as shown in Figure 9, a similar pattern was observed for MPRR, which increased with HVO content at the lower T_a, but decreased at the higher T_a. Some confirmation of the APRR results at the higher T_a can be found in the findings presented in [62], where pressure traces recorded in an engine cylinder showed that, for various injection strategies and EGR rates, HVO produced a smoother pressure rise in the phase between the SOI and the peak cylinder pressure.

 doi:10.20944/preprints202510.1264.v1

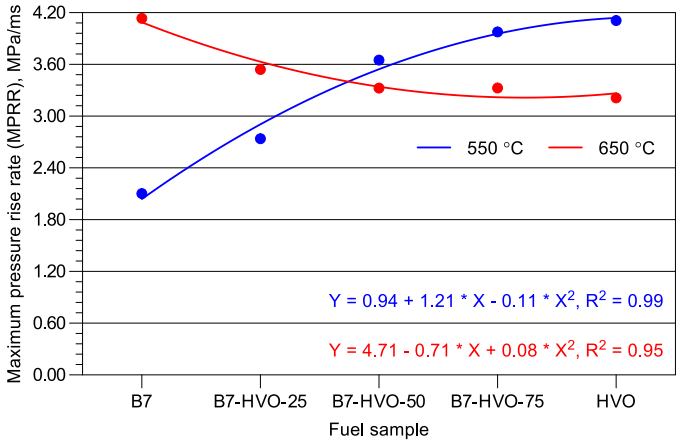

Figure 10. MPRR for B7, B7-HVO blends, and HVO at 550 °C and 650 °C.

As indicated by the pressure traces (Figure 5) and Equation (1), at the lower T_a, given the similar maximum pressure values inside the chamber across the tested samples, the interval between the point of peak pressure and the end of the ID period decreased as the HVO share in the fuel increased. This explains the observed drop in APRR and MPRR readings with rising HVO share at the lower T_a. At the higher T_a, this time difference also decreased slightly with increasing HVO content, which similarly resulted in a decline in the APRR and MPRR parameters.

Under constant volume combustion conditions, the pressure traces are directly reflected in the corresponding aHRR profiles, which were determined using the recorded pressure signal. The aHRR results for the tested fuel samples—presented as a supplement to the data describing autoignition behavior and combustion characteristics—are shown in Figure 11.

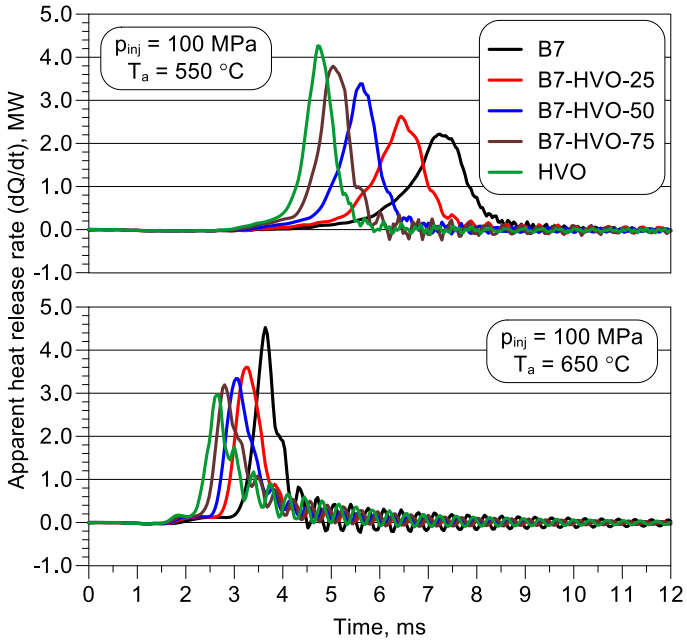

Figure 11. aHRR for B7, B7-HVO blends, and HVO at 550 °C and 650 °C.

As presented in Figure 11, at the lower of the two evaluated temperatures, T_a, despite the notable decrease in ID as the proportion of HVO in the diesel mixture increased, the heat release intensity increased, with the highest peak value recorded for neat HVO. This indicates a dominant effect of the higher reactivity of fuels associated with a greater proportion of paraffinic hydrocarbons. In this case, the reduced quantity of fuel involved during the early stage of premixed combustion, due to shorter

 doi:10.20944/preprints202510.1264.v1

ID, did not lead to a decrease in heat release intensity—as is typically observed for conventional fuels, which contain approximately 20–30% aromatic hydrocarbons by mass.

At the higher initial temperature, T_a, the trend in aHRR reversed: the highest heat release intensity was recorded for B7, and it progressively decreased as the proportion of HVO in the diesel blend increased, reaching its minimum value for neat HVO. This effect was associated with the reduced fuel mass participating in the early combustion phase, resulting from the shortened ID values. As previously mentioned, under higher initial chamber temperatures, both the chemical and physical aspects of ignition delay were shortened. Although the combustion conditions within a constant-volume chamber differ significantly from those inside an operating diesel engine, the data presented in Figure 11 for T_a = 650 °C are, to some extent, consistent with engine data reported in [62], where HVO exhibited a lower rate of heat release relative to diesel.

Based on the recorded values of ID and CD, the average DCN values were calculated in accordance with the procedure described in [34,35], and are presented in Figure 12. The DCN measured via the CVCC technique shows equivalence to the CN values obtained from engine-based procedures described in [21,22]. DCN analysis is particularly relevant in cases where the objective involves evaluating the ignition quality of a tested fuel sample against standardized criteria or with the specifications outlined in the Worldwide Fuel Charter (WWFC) [72].

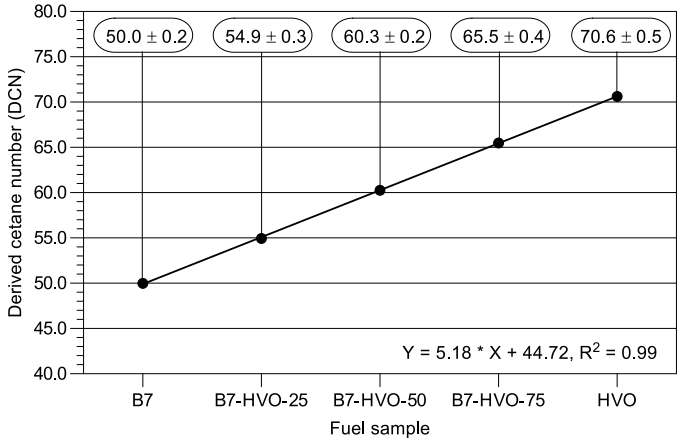

Figure 12. DCN for B7, B7-HVO blends, and HVO.

As shown in Figure 12, an increase in the proportion of HVO blended with B7 led to a linear rise in DCN. For the B7 sample, a DCN value of 50 was recorded, which is slightly below the minimum acceptable limit specified in [19] (min. 51). However, in terms of DCN, the B7 sample met the requirements for all diesel fuel categories defined in [20] (min. 40 and 30), as well as for Category 1 in the WWFC [72] (min. 48). Starting from the B7-HVO-25 blend, all tested samples comfortably met most of the requirements set by the referenced standards and the WWFC. Only the B7-HVO-25 sample did not meet the threshold for Categories 4 and 5 as defined in the WWFC (min. 55). It is important to recognize that DCN ratings would vary if different base fuels (i.e., B7 and HVO) were used. A similar linear increase in DCN with rising HVO content in diesel fuel was also reported by the authors of [51], who used the method described in [31] to determine DCN.

The experimental data presented in this section are complemented by an analysis of measurement uncertainty. The standard error of the mean (SEM) was used as the measure of uncertainty and was calculated for each data point based on six repetitions. Due to their small magnitude, the SEM values were not displayed as error bars in the graphs. Instead, they are listed in Tables 5 and 6, separately for each of the two analyzed temperatures. As noted in Section 2.3, SEM values for the measured parameters are indicated by the symbol Φ.

Table 5. Set and recorded fuel injection parameters and SEM values for the measured parameters at T_a = 550 °C.

 doi:10.20944/preprints202510.1264.v1

	ΦID [ms]	ΦCD [ms]	ΦAPRR [MPa/ms]	ΦMPRR [MPa/ms]	ΦMPR [MPa]	T_{ch} (T_a) [°C]	p_0 [MPa]	p_{inj} [MPa]	t_{inj} [ms]
B7	0.0560	0.0689	0.012	0.118	0.003	550.1	2.00	99.4	2.5
B7-HVO-25	0.0383	0.0582	0.023	0.107	0.004	549.8	1.99	99.2	2.5
B7-HVO-50	0.0354	0.0484	0.043	0.269	0.001	550.3	2.00	98.9	2.5
B7-HVO-75	0.0207	0.0305	0.048	0.092	0.180	540.2	2.00	99.5	2.5
HVO	0.0328	0.0304	0.062	0.144	0.021	550.2	1.99	99.3	2.5

Table 6. Set and recorded fuel injection parameters and SEM values for the measured parameters at T_a = 650 °C.

	ΦID [ms]	ΦCD [ms]	ΦAPRR [MPa/ms]	ΦMPRR [MPa/ms]	ΦMPR [MPa]	T_{ch} (T_a) [°C]	p_0 [MPa]	p_{inj} [MPa]	t_{inj} [ms]
B7	0.0090	0.0109	0.012	0.132	0.005	649.6	1.99	99.6	2.5
B7-HVO-	0.0129	0.0172	0.013	0.149	0.004	649.6	1.99	100.0	2.5
B7-HVO-	0.0118	0.0076	0.016	0.126	0.010	649.6	1.99	99.3	2.5
B7-HVO-	0.0182	0.0149	0.012	0.208	0.017	649.9	2.00	99.3	2.5
HVO	0.0110	0.0184	0.011	0.279	0.002	649.6	2.00	99.3	2.5

Tables 5 and 6 also include the average values of T_{ch}, p_0, and p_{inj}, which are set parameters in the adopted measurement methodology. With the exception of T_{ch}, the values of these parameters corresponded to the calibration settings defined in Table 4. The SEM values for DCN are presented in Figure 12, as they refer to the standardized measurement performed at $T_a = T_{ch}$ = 588 °C.

4. Conclusions

The conducted investigations of autoignition characteristics were performed using a constant-volume combustion chamber. Measurements involved a representative diesel fuel commercially available in Europe under the name B7 (indicating the maximum volumetric content of FAME), for HVO, and for blends of these fuels with HVO volumetric contents of 25%, 50%, and 75%. To enable a more comprehensive assessment of autoignition behavior—particularly for HVO and its blends with diesel—experiments were performed at two different initial chamber air temperatures: 550 °C and 650 °C. Several measurable parameters were used to characterize autoignition properties, including the DCN. The experimental setup used in this study included a high-pressure fuel injection system, representative of those used in current diesel engine injection systems. On the basis of these outcomes, the following insights and observations were established:

- An increase in the proportion of HVO within the diesel mixture resulted in a clear reduction in ID and CD, although these changes were significantly smaller at the higher initial temperature of the intake air into which the fuel was delivered.
- Increasing HVO share in the diesel mixture led to a rise in MPR at lower initial combustion chamber air temperature, with the most pronounced changes observed for the 75% HVO blend and neat HVO. At the higher initial chamber temperature, the HVO content in the blend had virtually no effect on the MPR value.
- The APRR parameter increased with rising HVO content at the lower initial combustion chamber temperature. However, at the higher temperature, APRR values were significantly lower and decreased as the HVO content increased. Under engine-like conditions, it may therefore be beneficial to inject fuel into a hotter combustion environment when operating on neat HVO or diesel–HVO fuel mixtures.

 doi:10.20944/preprints202510.1264.v1

- For the MPRR parameter, the trend was consistent with that observed for APRR; however, the differences in absolute values were smaller when comparing the two initial combustion chamber temperatures.
- At the lower of the two analyzed initial combustion chamber temperatures, despite a clear reduction in ID, as the proportion of HVO in the diesel mixture increased, the heat release intensity rose, with the highest peak value observed for neat HVO.
- At the higher initial combustion chamber temperature, the trend in aHRR was reversed: the highest heat release intensity was recorded for neat diesel fuel and decreased as HVO concentration in the blend rose, reaching its lowest value for neat HVO.
- A higher HVO share in the diesel mixture led to a linear increase of DCN.

The present study expands on the scarce data currently available regarding the quantitative evaluation of autoignition characteristics for neat HVO and its mixtures with regular diesel, as well as their comparison to those of a widely used commercial diesel. Applying a constant-volume combustion chamber and maintaining strict control over initial conditions at the moment of fuel injection enabled an accurate evaluation of autoignition performance in relation to only two key parameters: the initial combustion chamber temperature and the volumetric ratio of HVO to diesel. The results obtained may be useful for optimizing control strategies in fuel injection systems of diesel engines powered by HVO or HVO-diesel blends.

Author Contributions: Conceptualization, H.K.; methodology, H.K., A.J. and D.Sz.; software, H.K., A.J.; validation, H.K.; formal analysis, H.K.; investigation, H.K., A.J. and D.Sz.; resources, H.K., A.J. and D.Sz.; data curation, H.K., A.J. and D.Sz.; writing—original draft preparation, H.K.; writing—review and editing, H.K., A.J. and D.Sz.; visualization, H.K.; supervision, H.K., A.J. and D.Sz.; All authors have read and agreed to the published version of the manuscript.

Funding: The research leading to these results has received funding from the commissioned task entitled „VIA CARPATIA Universities of Technology Network named after the President of the Republic of Poland Lech Kaczyński", under the special purpose grant from the Minister of Science and Higher Education, contract no. MEiN/2022/DPI/2578 action entitled "In the neighborhood - inter-university research internships and study visits".

Data Availability Statement: Data are contained within the article.

Conflicts of Interest: The authors declare no conflicts of interest

Abbreviations

The following abbreviations are used in this manuscript:

HVO	Hydrotreated vegetable oil
ID	ignition delay
CD	combustion delay
APRR	average pressure rise rate
MPRR	maximum pressure rise rate
MPR	maximum pressure rise
aHRR	apparent heat release rate
NO_x	nitrogen oxide
CN	Cetane number
DCN	Derived cetane number
CVCC	constant volume combustion chamber
SOI	start of injection
EOI	end of injection
ULSD	ultra-low sulfur diesel
FAME	Fatty acid methyl esters
B7	diesel fuel with up to 7% (v/v) FAME, as per EN 590
2-EHN	2-Ethylhexyl nitrate

 doi:10.20944/preprints202510.1264.v1

HHV higher heating value
WSD wear scar diameter
IBP initial boiling point
FBP final boiling point
SEM standard error of the mean
T_a initial temperature inside the combustion chamber
T_{ch} chamber wall temperature
t_{inj} injector energized time
p_{inj} injection pressure
T_{co} injector nozzle coolant jacket temperature
Φ denotes the standard error of the mean associated with the respective parameter

References

1. I. Abrar and A. N. Bhaskarwar, "An overview of current trends and future scope for vegetable oil-based sustainable alternative fuels for compression ignition engines," Second and Third Generation of Feedstocks: The Evolution of Biofuels, pp. 531–556, Jan. 2019, doi: 10.1016/B978-0-12-815162-4.00019-7.
2. A. Sonthalia and N. Kumar, "Hydroprocessed vegetable oil as a fuel for transportation sector: A review," Journal of the Energy Institute, vol. 92, no. 1, pp. 1–17, Feb. 2019, doi: 10.1016/J.JOEI.2017.10.008.
3. G. A. A. da Costa, A. B. Mendes, and V. M. D. Silva, "Decarbonization pathways in Brazilian maritime cabotage: A comparative analysis of very low sulfur fuel oil, marine diesel oil, and hydrogenated vegetable oil in carbon dioxide equivalent emissions," Latin American Transport Studies, vol. 2, p. 100018, Dec. 2024, doi: 10.1016/J.LATRAN.2024.100018.
4. T. J. Hilbers, L. M. J. Sprakel, L. B. J. van den Enk, B. Zaalberg, H. van den Berg, and L. G. J. van der Ham, "Green Diesel from Hydrotreated Vegetable Oil Process Design Study," Chem Eng Technol, vol. 38, no. 4, pp. 651–657, Apr. 2015, doi: 10.1002/CEAT.201400648.
5. G. Lorenzi, L. Mignini, B. Venezia, C. Silva, and M. Santarelli, "Integration of high-temperature electrolysis in an HVO production process using waste vegetable oil," Energy Procedia, vol. 158, pp. 2005–2011, Feb. 2019, doi: 10.1016/J.EGYPRO.2019.01.465.
6. G. W. Huber, P. O'Connor, and A. Corma, "Processing biomass in conventional oil refineries: Production of high quality diesel by hydrotreating vegetable oils in heavy vacuum oil mixtures," Appl Catal A Gen, vol. 329, pp. 120–129, Oct. 2007, doi: 10.1016/J.APCATA.2007.07.002.
7. M. Pechout, M. Kotek, P. Jindra, D. Macoun, J. Hart, and M. Vojtisek-Lom, "Comparison of hydrogenated vegetable oil and biodiesel effects on combustion, unregulated and regulated gaseous pollutants and DPF regeneration procedure in a Euro6 car," Science of The Total Environment, vol. 696, p. 133748, Dec. 2019, doi: 10.1016/J.SCITOTENV.2019.133748.
8. N. A. Fathurrahman et al., "Long-term storage stability of incorporated hydrotreated vegetable oil (HVO) in biodiesel-diesel blends at highland and coastal areas," Fuel Communications, vol. 18, p. 100107, Mar. 2024, doi: 10.1016/J.JFUECO.2024.100107.
9. T. Bohl, A. Smallbone, G. Tian, and A. P. Roskilly, "Particulate number and NOx trade-off comparisons between HVO and mineral diesel in HD applications," Fuel, vol. 215, pp. 90–101, Mar. 2018, doi: 10.1016/J.FUEL.2017.11.023.
10. I. Bortel, J. Vávra, and M. Takáts, "Effect of HVO fuel mixtures on emissions and performance of a passenger car size diesel engine," Renew Energy, vol. 140, pp. 680–691, Sep. 2019, doi: 10.1016/J.RENENE.2019.03.067.
11. W. Ajeeb, D. M. Gomes, R. C. Neto, and P. Baptista, "Life cycle analysis of hydrotreated vegetable oils production based on green hydrogen and used cooking oils," Fuel, vol. 390, p. 134749, Jun. 2025, doi: 10.1016/J.FUEL.2025.134749.
12. R. Suarez-Bertoa et al., "Impact of HVO blends on modern diesel passenger cars emissions during real world operation," Fuel, vol. 235, pp. 1427–1435, Jan. 2019, doi: 10.1016/J.FUEL.2018.08.031.
13. F. Sihlovec, D. Vrtiška, and P. Šimáček, "The use of multivariate statistics and mathematically modeled IR spectra for determination of HVO content in diesel blends," Fuel, vol. 379, p. 132963, Jan. 2025, doi: 10.1016/J.FUEL.2024.132963.

 doi:10.20944/preprints202510.1264.v1

14. "UNE EN 15940:2024 Automotive fuels - Paraffinic diesel fuel from synthesis or hydrotreatment - Requirements and test methods." Accessed: Apr. 09, 2025. [Online]. Available: https://www.en-standard.eu/une-en-15940-2024-automotive-fuels-paraffinic-diesel-fuel-from-synthesis-or-hydrotreatment-requirements-and-test-methods/
15. C. Aligrot, J. C. Champoussin, N. Guerrassi, and G. Claus, "A correlative model to predict autoignition delay of diesel fuels," SAE Technical Papers, 1997, doi: 10.4271/970638.
16. M. Aldhaidhawi, L. Miron, R. Chiriac, and V. Badescu, "Autoignition Process in Compression Ignition Engine Fueled by Diesel Fuel and Biodiesel with 20% Rapeseed Biofuel in Diesel Fuel," Journal of Energy Engineering, vol. 144, no. 5, Oct. 2018, doi: 10.1061/(ASCE)EY.1943-7897.0000563.
17. M. Aldhaidhawi, R. Chiriac, and V. Badescu, "Ignition delay, combustion and emission characteristics of Diesel engine fueled with rapeseed biodiesel – A literature review," Renewable and Sustainable Energy Reviews, vol. 73, pp. 178–186, 2017, doi: 10.1016/j.rser.2017.01.129.
18. L. Miron, R. Chiriac, M. Brabec, and V. Bădescu, "Ignition delay and its influence on the performance of a Diesel engine operating with different Diesel–biodiesel fuels," Energy Reports, vol. 7, pp. 5483–5494, Nov. 2021, doi: 10.1016/J.EGYR.2021.08.123.
19. "BS EN 590:2013+A1:2017 Automotive fuels. Diesel. Requirements and test methods." Accessed: Apr. 09, 2025. [Online]. Available: https://www.en-standard.eu/bs-en-590-2013-a1-2017-automotive-fuels-diesel-requirements-and-test-methods/
20. "D975 Standard Specification for Diesel Fuel." Accessed: Apr. 09, 2025. [Online]. Available: https://store.astm.org/d0975-21.html
21. "ISO 5165:2020 - Petroleum products — Determination of the ignition quality of diesel fuels — Cetane engine method." Accessed: Apr. 09, 2025. [Online]. Available: https://www.iso.org/standard/76906.html
22. "D613 Standard Test Method for Cetane Number of Diesel Fuel Oil." Accessed: Apr. 09, 2025. [Online]. Available: https://store.astm.org/standards/d613
23. Y. Kidoguchi, C. Yang, R. Kato, and K. Miwa, "Effects of fuel cetane number and aromatics on combustion process and emissions of a direct-injection diesel engine," JSAE review, vol. 21, no. 4, pp. 469–475, 2000, doi: 10.1016/S0389-4304(00)00075-8.
24. E. Kurtz and C. J. Polonowski, "The Influence of Fuel Cetane Number on Catalyst Light-Off Operation in a Modern Diesel Engine," SAE Int J Fuels Lubr, vol. 10, no. 3, Aug. 2017, doi: 10.4271/2017-01-9378.
25. R. Cataluña and R. Da Silva, "Effect of Cetane Number on Specific Fuel Consumption and Particulate Matter and Unburned Hydrocarbon Emissions from Diesel Engines," Journal of Combustion, vol. 2012, no. 1, p. 738940, Jan. 2012, doi: 10.1155/2012/738940.
26. O. C. Chukwuezie, N. R. Nwakuba, S. N. Asoegwu, and K. N. Nwaigwe, "Cetane Number Effect on Engine Performance and Gas Emission: A Review," American Journal of Engineering Research (AJER), no. 6, pp. 56–67, 2017, Accessed: Apr. 09, 2025. [Online]. Available: www.ajer.org
27. J. Reijnders, M. Boot, and P. de Goey, "Impact of aromaticity and cetane number on the soot-NOx trade-off in conventional and low temperature combustion," Fuel, vol. 186, pp. 24–34, Dec. 2016, doi: 10.1016/J.FUEL.2016.08.009.
28. J. Yanowitz, E. M. A. Ratcliff, R. L. Mccormick, J. D. Taylor, and M. J. Murphy Battelle, "Compendium of Experimental Cetane Numbers," 2014, Accessed: Apr. 09, 2025. [Online]. Available: www.nrel.gov/publications.
29. A. D. B. Yates, C. L. Viljoen, and A. Swarts, "Understanding the Relation Between Cetane Number and Combustion Bomb Ignition Delay Measurements," SAE Technical Papers, Jun. 2004, doi: 10.4271/2004-01-2017.
30. T. W. Ryan, "Correlation of Physical and Chemical Ignition Delay to Cetane Number," SAE Technical Papers, Oct. 1985, doi: 10.4271/852103.
31. "D6890 Standard Test Method for Determination of Ignition Delay and Derived Cetane Number (DCN) of Diesel Fuel Oils by Combustion in a Constant Volume Chamber." Accessed: Apr. 09, 2025. [Online]. Available: https://store.astm.org/d6890-21.html
32. "UNE EN 15195:2023 Liquid petroleum products - Determination of ignition delay and derived cetane number (DCN) of middle distillate fuels by combustion in a constant volume chamber." Accessed: Apr. 09,

 doi:10.20944/preprints202510.1264.v1

2025. [Online]. Available: https://www.en-standard.eu/une-en-15195-2023-liquid-petroleum-products-determination-of-ignition-delay-and-derived-cetane-number-dcn-of-middle-distillate-fuels-by-combustion-in-a-constant-volume-chamber/

33. "CSN EN 16144 - Liquid petroleum products - Determination of ignition delay and derived cetane number (DCN) of middle distillate fuels - Fixed range injection period, constant volume combustion chamber method." Accessed: Apr. 09, 2025. [Online]. Available: https://www.en-standard.eu/csn-en-16144-liquid-petroleum-products-determination-of-ignition-delay-and-derived-cetane-number-dcn-of-middle-distillate-fuels-fixed-range-injection-period-constant-volume-combustion-chamber-method/
34. "BS EN 16715:2015 Liquid petroleum products. Determination of ignition delay and derived cetane number (DCN) of middle distillate fuels. Ignition delay and combustion delay determination using a constant volume combustion chamber with direct fuel injection." Accessed: Apr. 09, 2025. [Online]. Available: https://www.en-standard.eu/bs-en-16715-2015-liquid-petroleum-products-determination-of-ignition-delay-and-derived-cetane-number-dcn-of-middle-distillate-fuels-ignition-delay-and-combustion-delay-determination-using-a-constant-volume-combustion-chamber-with-direct-fuel-inj/
35. "D7668 Standard Test Method for Determination of Derived Cetane Number (DCN) of Diesel Fuel Oils—Ignition Delay and Combustion Delay Using a Constant Volume Combustion Chamber Method." Accessed: Apr. 09, 2025. [Online]. Available: https://store.astm.org/d7668-17.html
36. H. Kuszewski, A. Jaworski, A. Ustrzycki, K. Lejda, K. Balawender, and P. Woś, "Use of the constant volume combustion chamber to examine the properties of autoignition and derived cetane number of mixtures of diesel fuel and ethanol," Fuel, vol. 200, 2017, doi: 10.1016/j.fuel.2017.04.021.
37. H. Kuszewski, "'Experimental investigation of the effect of ambient gas temperature on the autoignition properties of ethanol–diesel fuel blends,'" Fuel, vol. 214, 2018, doi: 10.1016/j.fuel.2017.10.123.
38. M. Lapuerta, J. J. Hernández, D. Fernández-Rodríguez, and A. Cova-Bonillo, "Autoignition of blends of n-butanol and ethanol with diesel or biodiesel fuels in a constant-volume combustion chamber," Energy, vol. 118, pp. 613–621, Jan. 2017, doi: 10.1016/J.ENERGY.2016.10.090.
39. F. Millo et al., "A fundamental study of injection and combustion characteristics of neat Hydrotreated Vegetable Oil (HVO) as a fuel for light-duty diesel engines," Fuel, vol. 379, p. 132951, Jan. 2025, doi: 10.1016/J.FUEL.2024.132951.
40. K. O. P. Bjørgen, D. R. Emberson, and T. Løvås, "Combustion and soot characteristics of hydrotreated vegetable oil compression-ignited spray flames," Fuel, vol. 266, p. 116942, Apr. 2020, doi: 10.1016/J.FUEL.2019.116942.
41. J. Hunicz, M. Mikulski, P. C. Shukla, and M. S. Gęca, "Partially premixed combustion of hydrotreated vegetable oil in a diesel engine: Sensitivity to boost and exhaust gas recirculation," Fuel, vol. 307, 2022, doi: 10.1016/j.fuel.2021.121910.
42. M. Lapuerta, M. Villajos, J. R. Agudelo, and A. L. Boehman, "Key properties and blending strategies of hydrotreated vegetable oil as biofuel for diesel engines," Fuel Processing Technology, vol. 92, no. 12, pp. 2406–2411, Dec. 2011, doi: 10.1016/J.FUPROC.2011.09.003.
43. G. M. Pinto et al., "Hydrogen and CNG dual-fuel operation of a 6-Cylinder CI engine fueled by HVO and diesel: Emissions, efficiency, and combustion analyses," Int J Hydrogen Energy, vol. 111, pp. 407–432, Mar. 2025, doi: 10.1016/J.IJHYDENE.2025.02.306.
44. A. Dimitriadis et al., "Improving PM-NOx trade-off with paraffinic fuels: A study towards diesel engine optimization with HVO," Fuel, vol. 265, p. 116921, Apr. 2020, doi: 10.1016/J.FUEL.2019.116921.
45. L. F. A. Roque et al., "Experimental analysis and life cycle assessment of green diesel (HVO) in dual-fuel operation with bioethanol," J Clean Prod, vol. 389, p. 135989, Feb. 2023, doi: 10.1016/J.JCLEPRO.2023.135989.
46. A. Singer et al., "Aging studies of biodiesel and HVO and their testing as neat fuel and blends for exhaust emissions in heavy-duty engines and passenger cars," Fuel, vol. 153, pp. 595–603, Aug. 2015, doi: 10.1016/J.FUEL.2015.03.050.
47. C. Tan et al., "Investigation on Transient Emissions of a Turbocharged Diesel Engine Fuelled by HVO Blends," SAE Int J Engines, vol. 6, no. 2, pp. 1046–1058, Apr. 2013, doi: 10.4271/2013-01-1307.

 doi:10.20944/preprints202510.1264.v1

48. J. T. Bays et al., "Detailed Compositional Comparison of Hydrogenated Vegetable Oil with Several Diesel Fuels and Their Effects on Engine-Out Emissions," SAE Int J Fuels Lubr, vol. 16, no. 3, pp. 193–220, Dec. 2022, doi: 10.4271/04-16-03-0015.
49. C. Claudio, S. d'Ambrosio, M. Alessandro, M. Omar, and S. Nicolò, "Emissions, Performance and Vibro-Acoustic Analysis of a Compression-Ignition Engine Running on Hydrotreated Vegetable Oil (HVO)," American Society of Mechanical Engineers, Internal Combustion Engine Division (Publication) ICE, vol. 2024-October, Dec. 2024, doi: 10.1115/ICEF2024-140754.
50. D. Kim, S. Kim, S. Oh, and S. Y. No, "Engine performance and emission characteristics of hydrotreated vegetable oil in light duty diesel engines," Fuel, vol. 125, pp. 36–43, Jun. 2014, doi: 10.1016/J.FUEL.2014.01.089.
51. S. A. Alkhayat, G. D. Joshi, and N. Henein, "Analysis and Correlation of Ignition Delay for Hydrotreated Vegetable Oil and Ultra Low Sulfur Diesel and Their Blends in Ignition Quality Tester," Fuel, vol. 289, p. 119816, Apr. 2021, doi: 10.1016/J.FUEL.2020.119816.
52. J. J. Hernández, A. Cova-Bonillo, H. Wu, J. Barba, and J. Rodríguez-Fernández, "Low temperature autoignition of diesel fuel under dual operation with hydrogen and hydrogen-carriers," Energy Convers Manag, vol. 258, p. 115516, Apr. 2022, doi: 10.1016/J.ENCONMAN.2022.115516.
53. H. Kuszewski and A. Jaworski, "Investigating the Effect of 2-Ethylhexyl Nitrate Cetane Improver (2-EHN) on the Autoignition Characteristics of a 1-Butanol–Diesel Blend," Energies 2024, Vol. 17, Page 4085, vol. 17, no. 16, p. 4085, Aug. 2024, doi: 10.3390/EN17164085.
54. H. Kuszewski, "Experimental investigation of the autoignition properties of ethanol–biodiesel fuel blends," Fuel, vol. 235, 2019, doi: 10.1016/j.fuel.2018.08.146.
55. V. Soloiu et al., "Fischer-Tropsch coal-to-liquid fuel negative temperature coefficient region (NTC) and low-temperature heat release (LTHR) in a constant volume combustion chamber (CVCC)," Energy, vol. 198, p. 117288, May 2020, doi: 10.1016/J.ENERGY.2020.117288.
56. H. Kuszewski, "Effect of Injection Pressure and Air–Fuel Ratio on the Self-Ignition Properties of 1-Butanol–Diesel Fuel Blends: Study Using a Constant-Volume Combustion Chamber," Energy & Fuels, vol. 33, no. 3, pp. 2335–2347, Mar. 2019, doi: 10.1021/ACS.ENERGYFUELS.8B04523.
57. J. J. Hernández, A. Cova-Bonillo, A. Ramos, H. Wu, and J. Rodríguez-Fernández, "Autoignition of sustainable fuels under dual operation with H2-carriers in a constant volume combustion chamber," Fuel, vol. 339, p. 127487, May 2023, doi: 10.1016/J.FUEL.2023.127487.
58. H. Kuszewski, "Effect of adding 2-ethylhexyl nitrate cetane improver on the autoignition properties of ethanol–diesel fuel blend – Investigation at various ambient gas temperatures," Fuel, vol. 224, 2018, doi: 10.1016/j.fuel.2018.03.084.
59. M. Lapuerta, J. Sanz-Argent, and R. R. Raine, "Ignition Characteristics of Diesel Fuel in a Constant Volume Bomb under Diesel-Like Conditions. Effect of the Operation Parameters," Energy and Fuels, vol. 28, no. 8, pp. 5445–5454, Aug. 2014, doi: 10.1021/EF500535J.
60. X. Fu and S. K. Aggarwal, "Two-stage ignition and NTC phenomenon in diesel engines," Fuel, vol. 144, pp. 188–196, Mar. 2015, doi: 10.1016/J.FUEL.2014.12.059.
61. E. Rosseel and R. Sierens, "The Physical and the Chemical Part of the Ignition Delay in Diesel Engines," SAE Technical Papers, May 1996, doi: 10.4271/961123.
62. W. Szeto and D. Y. C. Leung, "Is hydrotreated vegetable oil a superior substitute for fossil diesel? A comprehensive review on physicochemical properties, engine performance and emissions," Fuel, vol. 327, p. 125065, Nov. 2022, doi: 10.1016/J.FUEL.2022.125065.
63. S. M. Heck, H. O. Pritchard, and J. F. Griffiths, "Cetane number vs. structure in paraffin hydrocarbons," Journal of the Chemical Society, Faraday Transactions, vol. 94, no. 12, pp. 1725–1727, Jan. 1998, doi: 10.1039/A800861B.
64. A. Mohammed Elbanna, C. Xiaobei, Y. Can, M. Elkelawy, H. Alm-Eldin Bastawissi, and H. Panchal, "Fuel reactivity controlled compression ignition engine and potential strategies to extend the engine operating range: A comprehensive review," Energy Conversion and Management: X, vol. 13, p. 100133, Jan. 2022, doi: 10.1016/J.ECMX.2021.100133.

 doi:10.20944/preprints202510.1264.v1

65. G. Floweday, "A New Functional Global Auto-ignition Model for Hydrocarbon Fuels - Part 1 of 2: An Investigation of Fuel Auto-Ignition Behaviour and Existing Global Models," SAE Int J Fuels Lubr, vol. 3, no. 2, pp. 710–724, Oct. 2010, doi: 10.4271/2010-01-2161.
66. H. J. Curran et al., "A Comprehensive Modeling Study of n-Heptane Oxidation," CoFl, vol. 114, no. 1, pp. 149–177, 1998, doi: 10.1016/S0010-2180(97)00282-4.
67. L. So Khuong, N. Hashimoto, Y. Konno, Y. Suganuma, H. Nomura, and O. Fujita, "Droplet evaporation characteristics of hydrotreated vegetable oil (HVO) under high temperature and pressure conditions," Fuel, vol. 368, p. 131604, Jul. 2024, doi: 10.1016/J.FUEL.2024.131604.
68. Y. Kidoguchi, Y. Nada, T. Ichikawa, H. Miyoshi, and K. Sakai, "Effect of Pilot Injection on Improvement of Fuel Consumption and Exhaust Emissions of IDI Diesel Engines," SAE Technical Papers, Jan. 2022, doi: 10.4271/2022-32-0013.
69. S. J. Yoon, B. Park, J. Park, and S. Park, "Effect of pilot injection on engine noise in a single cylinder compression ignition engine," International Journal of Automotive Technology, vol. 16, no. 4, pp. 571–579, Aug. 2015, doi: 10.1007/S12239-015-0058-6/METRICS.
70. H. M. Kim, W. J. Cho, and K. H. Lee, "Effect of injection condition and swirl on D.I. diesel combustion in a transparent engine system," International Journal of Automotive Technology, vol. 9, no. 5, pp. 535–541, Oct. 2008, doi: 10.1007/S12239-008-0063-0/METRICS.
71. K. Bhaskar, G. Nagarajan, and S. Sampath, "The Effects of Premixed Ratios on the Performance and Emission of PPCCI Combustion in a Single Cylinder Diesel Engine," Int J Green Energy, vol. 10, no. 1, pp. 1–11, Jan. 2013, doi: 10.1080/15435075.2011.647364.
72. "Worldwide Fuel Charter 2019 - Gasoline and diesel fuel - ACEA - European Automobile Manufacturers' Association." Accessed: Apr. 14, 2025. [Online]. Available: https://www.acea.auto/publication/worldwide-fuel-charter-2019-gasoline-and-diesel-fuel/